Experimental Determination of the $NH_4NO_3/(NH_4)_2SO_4/H_2O$ Phase Diagram

Jameson R. Bothe and Keith D. Beyer*

Department of Chemistry, University of Wisconsin−La Crosse, La Crosse, Wisconsin 54601

Received: July 31, 2007; In Final Form: September 18, 2007

We have studied the thermodynamic properties of the ammonium nitrate/ammonium sulfate/water system using differential scanning calorimetry and infrared spectroscopy of thin films at low temperatures. This is the first study focused on low temperatures, as previous experimental work on this system has been at 273 K and above. We have combined our experimental results with melting point data from the literature at high temperatures to create a solid/liquid phase diagram of the ammonium nitrate/ammonium sulfate/water system for temperatures below 343 K. Using phase diagram theory and Alkemade lines, we predict which solids are stable at equilibrium for all concentrations within the studied region. We also observed the decomposition of a solid at low temperatures which has not previously been reported. Finally, we have compared our predicted solids and final melting temperatures to the Aerosol Inorganics Model (AIM).

Introduction

Tropospheric aerosols are predominantly made up of aqueous ammonium and sulfate ions with the molar ratio of NH_4^+/SO_4^{2-} ranging from 0 to 2.[1,2] Also, it has been shown that aerosols can contain a high content of nitrate ions.[2] Observations during the subsonic aircraft: contrail and cloud effects special study (SUCCESS) revealed free tropospheric aerosols containing significant amounts of NH_4^+, NO_3^-, and SO_4^{2-} including conditions where cirrus ice was present.[3] Also, theoretical[4,5] and laboratory[6−9] studies have shown the importance of ammoniated sulfate aerosols in cirrus cloud formation. Thus, the entire range of concentrations from dry $NH_4NO_3/(NH_4)_2SO_4$ particles (of varying ratios) to very dilute solutions may be possible in the atmosphere.[10] These particles absorb and scatter solar radiation dependent upon their phase, thus contributing to the radiation balance.[11,12] Therefore, the phase of the aerosol (aqueous or solid) contributes to its ability to scatter and absorb solar radiation. The particles may also play a significant role in heterogeneous chemistry in the troposphere.[13] More specifically, the probability of N_2O_5 hydrolysis occurring on the surface of an aerosol containing nitrate is a magnitude smaller than that of an aerosol composed of ammonium sulfate.[14] In all of these cases, understanding the thermodynamic properties at low temperatures is critical to knowing which phases may be present when particles crystallize and at what temperature solids will melt or dissolve into solution. However, it is understood that the phase diagram applicability to atmospheric aerosols assumes equilibrium has been established, and that the aerosols are not in metastable states. Equilibrium phase diagrams can be used as a starting point in predicting which phases may be present when aerosols freeze, because they give the most thermodynamically stable state for a given set of equilibrium conditions.

The phase diagram of the $NH_4NO_3/(NH_4)_2SO_4/H_2O$ ternary system has been previously studied above 273 K; it has been constructed from solubility data.[15−17] Two double salts, $2NH_4NO_3\cdot(NH_4)_2SO_4$ (2AN·AS) and $3NH_4NO_3\cdot(NH_4)_2SO_4$ (3AN·AS), exist as part of the $NH_4NO_3/(NH_4)_2SO_4$ binary system. However, primary phase fields of these solids in the aqueous ternary system have not been studied at low temperatures. Additionally, there is a possibility that unknown ternary solids exist at low temperatures. The lack of experimental work at low temperatures, which reflect those of the upper troposphere, invites investigation of the thermodynamics of this ternary system.

To study ternary systems, one must know the binary systems that comprise the ternary system well to effectively identify solids that may form. Additionally, ternary solids may form, which then makes knowledge of the stable binary solids extremely important in order to discern between known and new solids. The phase diagrams of the $(NH_4)_2SO_4/H_2O$ and NH_4NO_3/H_2O systems are well-known.[15−17] Also, limited melting point data exists for the $(NH_4)_2SO_4/NH_4NO_3$ binary system.[18,19] Here, we report the results of our investigation of the $NH_4NO_3/(NH_4)_2SO_4/H_2O$ system, primarily consisting of low-temperature data. We have coupled our experimental data with literature data to construct a ternary phase diagram, parametrize our melting point data, and compare our results to the predictions of the Aerosol Inorganics Model (AIM).[20]

Experimental Section

Sample Preparation. Ternary samples were prepared by mixing 99 wt % ACS reagent grade $(NH_4)_2SO_4$ and 99.5 wt % ACS reagent grade NH_4NO_3 supplied by Aldrich with deionized water. The concentration of all samples is known to ±0.40 wt %. The 3AN·AS salt was prepared by following the technique specified in method I found in Smith.[21] This method called for a salt mixture with an $NH_4NO_3/(NH_4)_2SO_4$ molar ratio of 6 to 1. The salt mixture was placed into a test tube with scratched walls, and water was added while maintaining a saturated mixture. The mixture was slowly heated until the water began to boil. More water was then added until all of the salt crystals had completely dissolved. The test tube was placed into a beaker filled with cool water and was allowed to sit overnight. The next day, the crystals were vacuum filtered from the solution and placed into a desiccator to dry. The dried salt was then used for ion and spectral analysis for comparison with the crystals that formed from $NH_4NO_3/(NH_4)_2SO_4/H_2O$ solutions.

* To whom correspondence should be addressed. E-mail: Beyer.Keit@uwlax.edu.

10.1021/jp0760859 CCC: $37.00
Published on Web 11/10/2007

Infrared Spectra. The sample cell used for infrared spectra is shown schematically and explained in detail in previous literature.[22] Briefly, a small drop of ternary solution was placed between two ZnSe windows, which were held in the center of an aluminum block by a threaded metal ring. Sample volumes were approximately 2 μL. On each side of the aluminum block, a Pyrex cell was purged with dry nitrogen gas. KBr windows were placed on the end of each cell, sealed with O-rings, and held in place by metal clamps. Heat tape was wrapped around the purge cells to prevent condensation on the KBr windows. The sample was cooled by pouring liquid nitrogen into a circular aluminum cup attached to the top of the main cell. The cell block was warmed by resistive heaters connected to a temperature controller. Temperature was measured by a copper constant and thermocouple placed at the edge of the ZnSe windows and connected to the temperature controller. The temperature of the cell was calibrated using Culligan purified water and high purity organic solvents (Aldrich): decane, octane, and acetic anhydride of which the melting points are 243.5, 216.4, and 200.2 K, respectively.[23] The IR cell temperatures are known on average to within $\pm$1.3 K, i.e., the temperature we measured in the IR cell of a specific transition is within 1.3 K of the transition temperature we measure (of the same transition) using the DSC.

Spectra were obtained with a Bruker Tensor 37 FTIR with an MCT-B detector at 4 cm^{-1} resolution. Each spectrum was the average of 10 scans. Before spectra were taken of a sample, a background scan was obtained from a dry, purged sample cell. Samples were cooled to 195 K at 3 K/min, and then allowed to warm to room temperature without resistive heating; typically, this was 1 K/min. Reference spectra for ammonium nitrate, ammonium sulfate, and 3AN·AS were obtained by making KBr pellets, 7 mm in diameter, containing each respective salt. The KBr used to make the salt pellets was 99 wt% FT-IR grade KBr supplied by Aldrich. Our spectra compare well for ice,[24] ammonium sulfate,[25] and ammonium nitrate.[25] Our spectra are not in full agreement with peak assignments for 3AN·AS that have been made in a previous study.[26] These differences are more extensively explained in the "Identification of Solids with FTIR" section.

Differential Scanning Calorimeter. Thermal data were obtained with both a Mettler Toledo DSC 822e with liquid nitrogen cooling and a Mettler Toledo DSC 822e cooled via an intra cooler. Each DSC utilized an HSS7 sensor. Industrial grade nitrogen gas was used as a purge gas with a flow rate of 50 mL/min. The temperature reproducibility of these instruments is better than $\pm$0.05 K. Our accuracy is estimated to be $\pm$0.9 K, with a probability of 0.94 based on a four point temperature calibration[27] using indium, HPLC grade water, anhydrous, high purity (99%+) octane, and anhydrous, high purity heptane (99%+) from Aldrich, the latter three stored under nitrogen. The sensitivity of our instrument to thermal signals is high. Previously, we calculated our sensitivity to detecting a component undergoing a thermal transition to be $<$50 ppm by mass, using the FRS5 sensor. Tests in our lab have shown the HSS7 is about seven times more sensitive.

Samples were contained in a 40 μL aluminum pan and typically had a mass of approximately 5 mg. We found that the best thermograms for determining final dissolution temperatures consisted of samples with solution volumes of 2 or 5 μL. Each sample was weighed before and after the experiment using a Mettler-Toledo AT20 microgram balance. The average mass loss from evaporation during the experiment was less than 1%. A typical sample was cooled to 183 K at 10 K per minute, held at that temperature for 5 min, and then warmed at a rate of 1 K per minute to a temperature at least 5 K above the predicted melting point.

Ion Chromatograph. Ion composition measurements of the 3AN·AS double salt formed by following method I in Smith et al.[21] were carried out using a Dionix ICS-90 ion chromatograph. All solutions were prepared using the salts dissolved in 18.2 MΩ Millipore filtered water. A column for anion analysis was utilized to measure the concentrations of NO_3^- and SO_4^{2-} in solution. Standard curves were produced for both NO_3^- and SO_4^{2-} using solutions with known NO_3^- and SO_4^{2-} concentrations and their respective peak areas in the chromatogram. The 3AN·AS salt was then used to prepare a solution to be run in the ion chromatograph. The calibration plots for NO_3^- and SO_4^{2-} were utilized to determine the concentrations of NO_3^- and SO_4^{2-} in the 3AN·AS solution in order to calculate the NO_3^-/SO_4^{2-} ratio in the salt.

Results

NH_4NO_3/H_2O and $(NH_4)_2SO_4$. To construct the $NH_4NO_3/(NH_4)_2SO_4/H_2O$ ternary phase diagram, both aqueous binary systems, NH_4NO_3/H_2O and $(NH_4)_2SO_4/H_2O$, needed to be well-known. We have previously studied the $(NH_4)_2SO_4/H_2O$ system and found excellent agreement with literature data.[28] Additionally, we experimentally investigated the NH_4NO_3/H_2O system and are in good agreement with the literature.[15,16] The eutectic melting temperature for the NH_4NO_3/H_2O system was found to be 255.56 $\pm$ 0.59 K, which compares well with the literature value of 256.35 K.[17]

$NH_4NO_3/(NH_4)_2SO_4/H_2O$. Figure 1 shows the concentrations of the data points from our experiments and the literature[9] that were used to construct the temperature contour ternary phase diagram. We studied a total of 175 samples, and a list of all of the samples with their respective concentrations and melting points can be found in Table 1S (see Supporting Information). We are unaware of any experimental data in the literature for temperatures below 273 K; therefore, the primary focus of our study consisted of mapping the unknown ice region and focusing on low-temperature transitions. The solubility data found in Silcock[15] ranges from 273 to 343 K; therefore, the ternary phase diagram reported here should be accurate from 343 K to low temperatures which reflect those of the upper troposphere. The temperature contour phase diagram for this system is found in Figure 2.

As shown in Figures 1 and 2, there are significant gaps in the solubility data of Silcock,[15] especially at high temperatures and low ammonium sulfate concentration. Therefore, uncertainty in the salt saturation temperature is greater in this region than in the rest of the phase diagram. No solubility data exists above 343 K; therefore, the region with temperatures above 343 K is unknown. We are unable to perform DSC and FTIR experiments at these high temperatures because of the significant water evaporation rate, which makes it difficult to prepare bulk samples with known concentrations. We also observe significant mass loss from DSC samples at these high temperatures, making the thermal data inaccurate. It was also difficult to determine the salt saturation temperature of samples that consisted of a significant ammonium sulfate weight fraction using DSC, as the dissolution enthalpy of ammonium sulfate is low. However, the dissolution enthalpy of ammonium nitrate is larger than that for ammonium sulfate; therefore, we had much more success determining the salt saturation temperatures of samples that consisted of 20 wt % ammonium nitrate and above. The concentrations used for experiments were chosen to maintain a

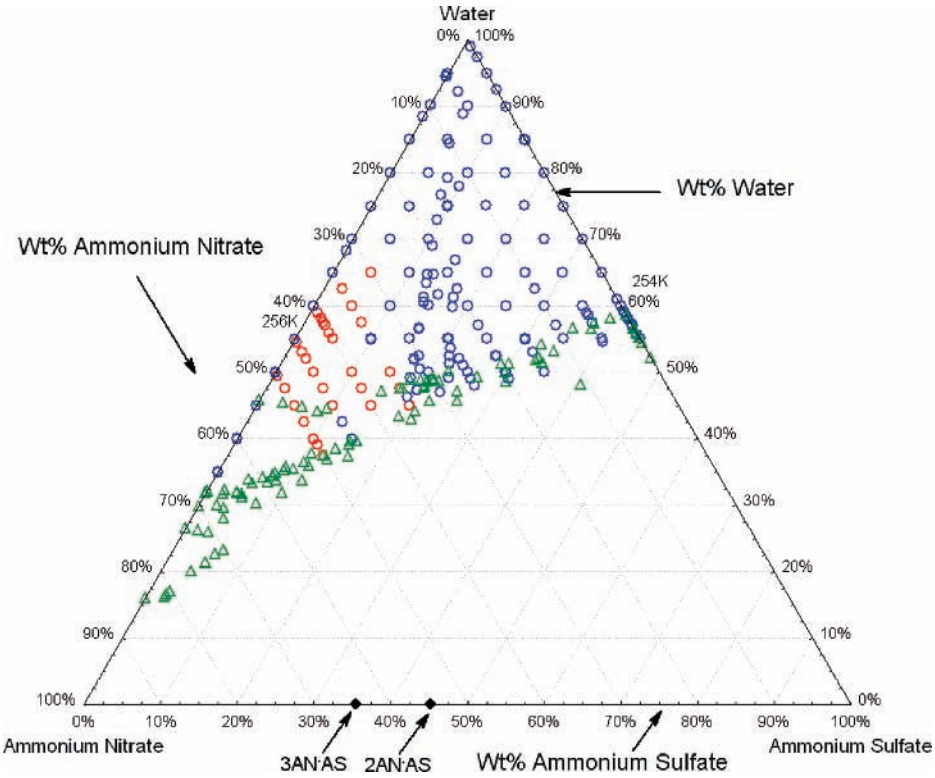

Figure 1. Data used to construct the $NH_4NO_3/(NH_4)_2SO_4/H_2O$ ternary phase diagram. The blue and red circles represent our experimental data points (the red circles are samples that displayed an additional solid decomposition of undetermined identity); the green triangles consist of solubility data found in Silcock.[15] Concentrations on ternary phase diagrams in this paper are read the following way: water concentrations are read horizontally using the scale on the right side of the diagram, NH_4NO_3 concentrations are read 120° from horizontal using the scale on the left side of the diagram, $(NH_4)_2SO_4$ concentrations are read 60° from horizontal using the scale at the bottom of the diagram.

TABLE 1: Phase Boundary Concentrations (wt %) and Temperatures as Determined from DSC and IR Experiments

wt % NH_4NO_3	wt % $(NH_4)_2SO_4$	wt % H_2O	phase boundary melt (K)	phase boundary solids[a]
5.0	35.5	59.5	254	ice/AS
10.0	30.0	60.0	254	ice/AS
15.0	27.5	57.5	252	ice/AS
20.0	20.3	59.7	253.5	ice/3AN·AS
25.0	15.9	59.1	253.4	ice/3AN·AS
30.0	14.0	56.0	250.3	ice/3AN·AS
35.0	8.6	56.4	254.1	ice/AN
40.0	2.0	58.0	256.6	ice/AN
45.0	10.1	44.9	272.4	AN/3AN·AS
50.0	10.0	40.0	280.7	AN/3AN·AS

[a] AS = $(NH_4)_2SO_4$, AN = NH_4NO_3, 3AN·AS = $3NH_4NO_3$·$(NH_4)_2SO_4$.

constant weight fraction of NH_4NO_3; consequently, we mapped the ternary phase diagram with constant weight fraction cross sections. These cross sections allowed the ice and salt primary phase fields to be mapped. Additionally, the cross-sections were used to map the location of the ice/salt phase boundary, since it appears as a temperature minimum in the cross section plots [see Figure 3 for examples]. The phase boundary compositions that were determined from the constant ammonium nitrate cross sections are found in Table 1. These compositions were used to draw the phase boundary in Figure 2 (indicated by a solid black line). We fit the final melting points of each cross-section to a second-order polynomial with the form:

$$T = A_2X^2 + A_1X + A_0 \quad (1)$$

where T is the final melting or saturation temperature, and X is the concentration (wt %) of ammonium sulfate with the concentration of ammonium nitrate held constant. A typical plot of this analysis is given for three cases in Figure 3. The constants for the parametrization in eq 1 are found in Table 2.

Our parametrization in the ice primary phase field models our experimental observations well, with an average deviation of ±1.0 K. The parametrizations provided for regions where the dissolution of a salt is the final transition have an average deviation of ±0.9 K from our experimental data; therefore, our parametrizations are within the experimental accuracy of the data. Although it was not the aim of this work, we did study 10 samples which had concentrations that matched those found in Silcock,[15] in order to compare our observed saturation temperatures with theirs. From the samples we ran, five had thermal signals strong enough to determine the final dissolution temperature. These data, with a comparison to Silcock, are given in Table 3. We found an average difference of 1.0 ± 0.7 K between our data and those of Silcock, thus showing good agreement with the historical data.

Ternary Eutectics. The phase boundary analysis described above leads to the discovery of invariant points in the phase diagram. These points are labeled with capital letters in Figure 4 and identified in Table 4. Two ternary eutectics are identified: NH_4NO_3/3AN·AS /H_2O (point A in Figure 4) and 3AN·AS /$(NH_4)_2SO_4/H_2O$ (point B in Figure 4). The temperature of each ternary eutectic is close to the temperature of the two binary eutectics and to each other as shown in Table 4. However, the melting paths of ternary samples can be used to determine the location of both ternary eutectic points. Their composition was determined using the temperatures of phase boundary transitions of many samples. Ternary eutectic points are temperature minimums on intersecting phase boundaries; thus, the temperature depression of the ice/salt phase boundary can be used to locate ternary eutectic compositions. An investigation of the

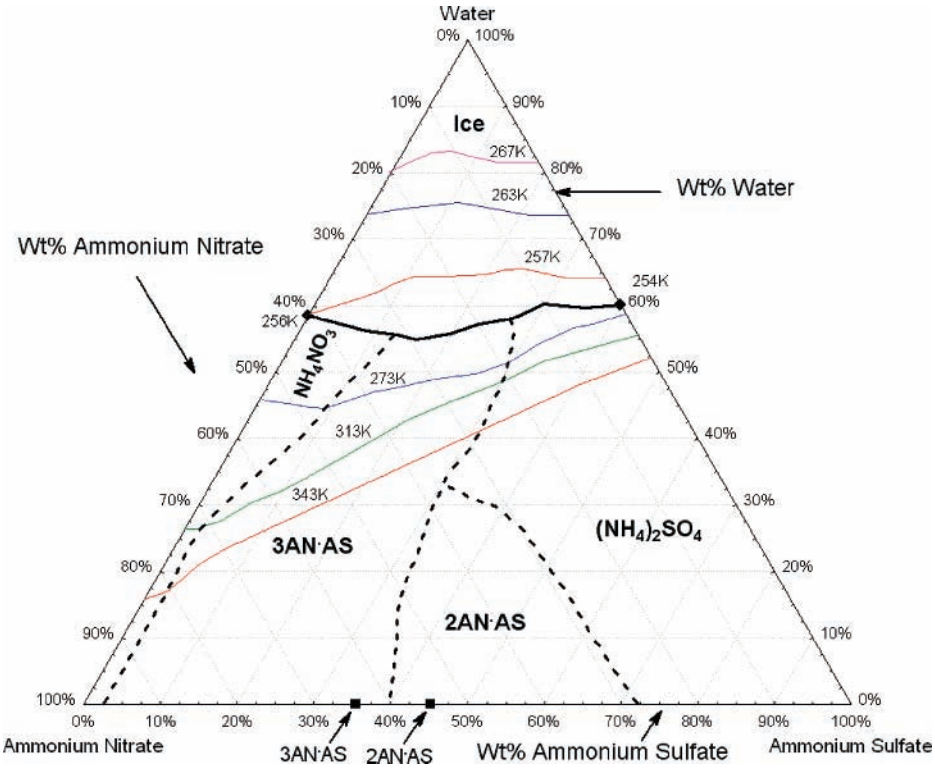

Figure 2. Temperature contour ternary phase diagram of the $NH_4NO_3/(NH_4)_2SO_4/ H_2O$ system constructed from our experimental data and the solubility data found in Silcock.[15] The thin colored lines are isotherms for the temperatures as labeled. The thick black line indicates the phase boundary between ice and the respective salts as given in the figure. The dashed lines speculate the location of the phase boundary that exists between NH_4NO_3/3AN·AS, 3AN·AS/$(NH_4)_2SO_4$, 3AN·AS /2AN·AS, and 2AN·AS/$(NH_4)_2SO_4$.

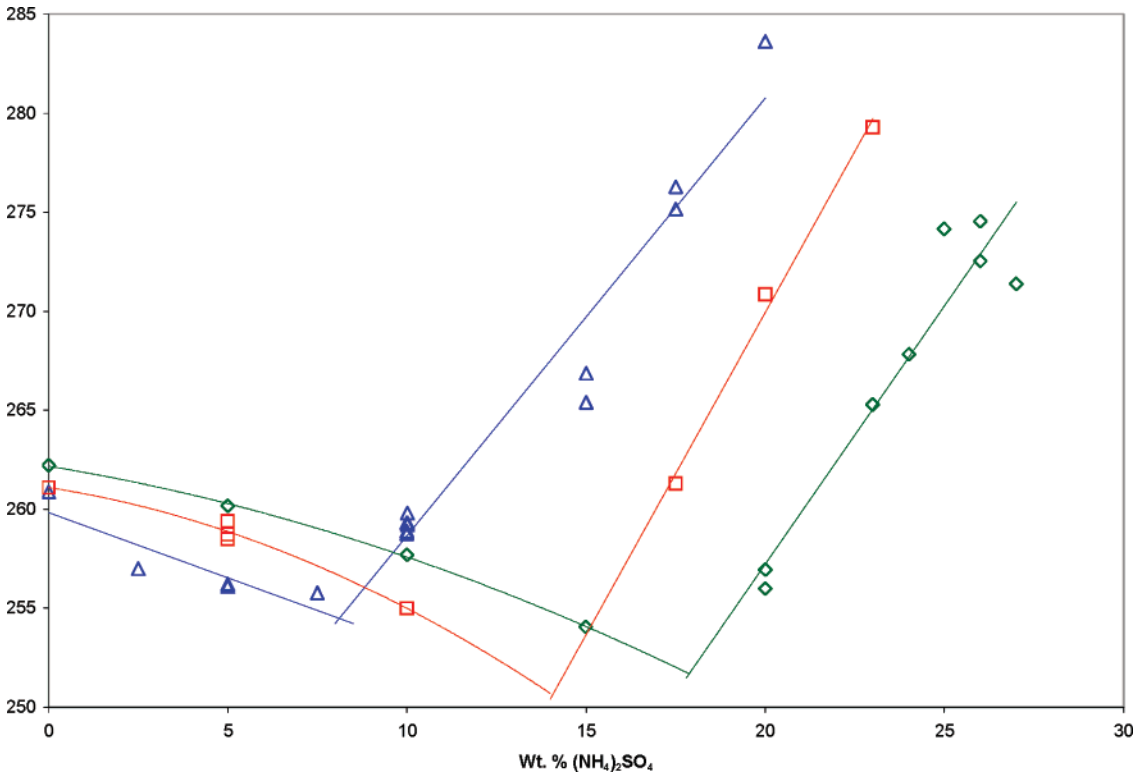

Figure 3. Plot of final melting/dissolution temperatures and concentrations of 25 (green diamonds and lines), 30 (red squares and lines), and 35 (blue triangles and lines) wt % NH_4NO_3, respectively. These are typical analyses which were performed for constant NH_4NO_3 concentrations in the range from 0 to 40 wt % $(NH_4)_2SO_4$.

ice/salt phase boundary around points A and B provides insight into their existence and location. If points A and B are both ternary eutectic compositions, then the following should occur on the phase boundary around points A and B: the phase boundary temperature should increase on both the ammonium sulfate poor and rich sides of each point. This increase in phase boundary temperature around each point indicates that it is a minimum and therefore a ternary eutectic.

TABLE 2: Melting Point Polynomial Coefficients for Eq 1

$[NH_4NO_3]$	A_2	A_1	A_0	valid $[(NH_4)_2SO_4]$
		Ice Primary Phase Region		
5	−0.0078	−0.2233	271.52	0.0−35.0
10	−0.0101	−0.2407	269.13	0.0−27.5
15	−0.0038	−0.4207	267.33	0.0−25.0
20	−0.0107	−0.3774	266.73	0.0−20.0
25	−0.0162	−0.2972	262.17	0.0−15.0
30	−0.0406	−0.204	261.09	0.0−10.0
35	0	−0.66	259.83	0.0−7.5
40	0	−1.1	258.85	0.0−2.0
		Salt Primary Phase Region		
20	0	1.3837	225.33	25.0−31.0
25	0	1.8868	223.47	23.0−27.0
30	0	3.2529	204.86	17.5−23.0
35	0	2.2123	236.52	10.0−20.0
40	0.0669	0.6195	256.58	2.5−17.0
45	−0.0591	1.6155	262.51	0.0−10.0
45	−0.1728	9.168	197.92	10.0−15.0
50	−0.0618	1.8397	268.45	0.0−10.0

TABLE 3: Our Experimental Data Compared to Solubility Found in Silcock[15]

wt % NH_4NO_3	wt % $(NH_4)_2SO_4$	wt % H_2O	exp. (K)	Silcock (K)
56.18	8.5	35.32	300	298
58.05	8.22	33.73	304	303
49.8	13.27	36.93	303	303
49.13	6.00	44.87	273.81	273
24.00	26.65	49.35	274.28	273

The thermograms in Figure 5 are used to show that ternary eutectic point A exists in Figure 4; additionally, the corresponding location of where each sample reaches the ice/salt phase boundary is indicated by the colored dashed lines in Figure 4. The green thermogram in Figure 5 with a composition of 20.00/7.50 wt % $NH_4NO_3/(NH_4)_2SO_4$ has ternary eutectic and phase boundary temperatures of 252.8 and 255.0 K, respectively. The phase boundary temperature of the green thermogram indicates the phase boundary is approaching a minimum by the decrease in temperature from the NH_4NO_3/H_2O binary eutectic temperature of 255.6 K; also, the ternary eutectic temperature of the green thermogram corresponds to the temperature of ternary eutectic point A in Figure 4. The brown thermogram in Figure 5, with a composition of 19.99/9.00 wt % $NH_4NO_3/(NH_4)_2SO_4$, has ternary eutectic and phase boundary temperatures of 252.8 and 254.6 K, respectively. The sample in the brown thermogram reaches the phase boundary on the opposite side of point A with respect to the green thermogram and shares the eutectic melting temperature corresponding with point A; yet, it also shares the phase boundary temperature of the green thermogram. This similarity in phase boundary temperature, between the green and brown thermograms, indicates that a minimum exists on the ice/salt phase boundary between the points where the melting paths of samples with concentrations of 20.00/7.50 and 19.99/9.00 wt % $NH_4NO_3/(NH_4)_2SO_4$ intersect the ice/salt phase boundary.

The blue thermogram in Figure 5, with a composition of 14.99/9.99 wt % $NH_4NO_3/(NH_4)_2SO_4$, has ternary eutectic and phase boundary temperatures of 250.9 and 253.6 K, respectively. The phase boundary temperature of the blue thermogram is lower than that of the brown thermogram; thus indicating that another minimum is being approached along the ice/salt phase boundary. Also, the blue thermogram's ternary eutectic melting temperature corresponds to the temperature of point B. The red thermogram in Figure 5, with a composition of 10.01/10.01 wt % $NH_4NO_3/(NH_4)_2SO_4$, has ternary eutectic and phase boundary temperatures of 250.8 and 252.4 K, respectively. Once again, the phase boundary temperature decreases as point B is approached along the phase boundary when comparing the phase boundary melts of the blue and red thermograms. Finally, the gray thermogram in Figure 5, with a composition of 5.01/36.02 wt % $NH_4NO_3/(NH_4)_2SO_4$, has ternary eutectic and phase boundary temperatures of 250.7 and 254.3 K, respectively. The phase boundary temperature of the gray thermogram is greater than that of the red thermogram; thus indicating that a temperature minimum, point B, exists between the points where the melting paths of samples with concentrations of 10.01/10.01 and 5.01/36.02 wt % $NH_4NO_3/(NH_4)_2SO_4$ intersect the ice/salt phase boundary.

It was a challenge to identify the location of the phase boundaries between the salts (dashed lines in Figures 2 and 4). As explained above, thermal signals in the DSC were quite weak in this region, which made it difficult to accurately determine the temperatures of phase boundary transitions and compositions between two salts. Also, the temperature difference between the aqueous binary eutectics and the ternary eutectics is very small, as shown in Table 4. This "flat" slope from the binary to ternary eutectic makes it difficult to discern the ternary eutectic signal from the melting signal along the phase boundary. It is difficult to determine which solids, other than 3AN·AS, are present in the sample using spectroscopy because 3AN·AS shares peaks with both ammonium nitrate and ammonium sulfate as is discussed in the Identification of Solids with FTIR section. The result of these challenges is that the uncertainty of the composition of solution at the two ternary eutectics is higher than we reported for other ternary systems and than we typically determine for binary eutectics in binary systems.[28]

Alkemade Lines. Once the phase boundaries are known in a ternary system, Alkemade lines can be drawn between molecular solid compositions that share a phase boundary.[29] These Alkemades, which can be viewed as binary cross-sections, constitute either a true or a pseudo-binary system. The Alkemade will be a true binary system if the Alkemade line intersects the common phase boundary between the binary solids. The Alkemade is a pseudo-binary if it does not intersect the common phase boundary between the binary solids. Alkemade lines divide a ternary system into ternary "subsystems", which can be studied independently of the overall system. Since these Alkemade subsystems constitute true ternary systems, each must have an invariant point, either within the Alkemade subsystem (a ternary eutectic) or outside the Alkemade subsystem (a tributary reaction point). Two combined molecular solids exist in the $NH_4NO_3/(NH_4)_2SO_4$ system: 2AN·AS and 3AN·AS. Therefore, theoretically, there could be Alkemade lines between each salt, 2AN·AS or 3AN·AS, and water.

We have experimentally shown that two invariant points, both of which are ternary eutectics, exist in this system. The presence of these two invariant points indicates that two unique Alkemade subsystems exist; therefore, an Alkemade line must exist between 3AN·AS /H_2O or 2AN·AS/H_2O. From our data and phase diagram theory, we have determined that 3AN·AS and water constitute a true binary system. The binary character of the 3AN·AS /H_2O system indicates that an Alkemade line exists between 3AN·AS and water.

Samples were analyzed using DSC and infrared spectroscopy with concentrations that fell on the 3AN·AS /H_2O Alkemade line. Both DSC and infrared spectroscopy experiments indicated that 3AN·AS is a true binary system. Each technique showed two transitions: the melting of ice and the dissolution of 3AN·AS. DSC thermograms of samples that are on the 3AN·AS /H_2O Alkemade line can be found in Figure 6. The transitions in the

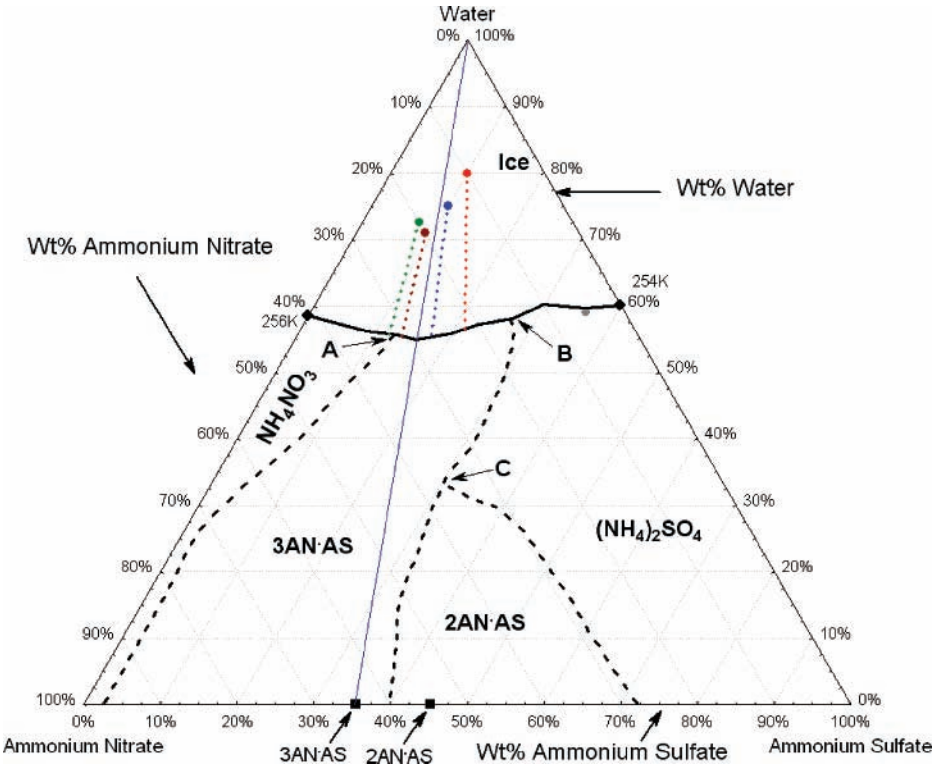

Figure 4. Ternary phase diagram that shows the Alkemade (blue) line between 3AN·AS and water. The large colored dots correspond to the concentration of samples for which thermograms are given in Figure 5 (same color). The corresponding colored dotted lines represent the liquid concentration path as the sample melts while heating. Thermal signals along this path are given in Figure 5.

TABLE 4: Phase Diagram Invariant Points as Given in Figure 4

wt % NH_4NO_3	wt % $(NH_4)_2SO_4$	T (K)	label in Figure 4	solids at invariant point	type of invariant point
32 ± 2	13 ± 2	252.53 ± 0.37	A	NH_4NO_3, 3AN·AS, H_2O	ternary eutectic
16 ± 2	26 ± 2	251.11 ± 0.48	B	3AN·AS, $(NH_4)_2SO_4$, H_2O	ternary eutectic
			C	3AN·AS, 2AN·AS, $(NH_4)_2SO_4$	tributary reaction point
41.52 ± 0.4	0	255.56 ± 0.59	D	ice, NH_4NO_3	binary eutectic
0	38.9 ± 0.4	254.71 ± 0.88	E	ice, $(NH_4)_2SO_4$	binary eutectic

blue thermogram are the melting of 3AN·AS and ice at 252.5 and 262.5 K, respectively. The transitions in the green thermogram are the melting of 3AN·AS and ice at 252.6 and 258.4 K, respectively. As is seen by the final melting temperatures of the blue and green thermograms, the melting point of ice is depressed as the concentration of 3AN·AS increases. The transitions in the red thermogram consist of the melting of ice and the dissolution of 3AN·AS at 252.5 and 281.9 K, respectively. The binary phase diagram for 3AN·AS/H_2O is included in Figure 7, and the eutectic temperature (average of 17 samples) is 252.52 ± 0.10 K. The binary eutectic temperature in Figure 7 is very close to the ternary eutectic temperature of ice/NH_4-SO_4/3AN·AS (point A) in Figure 3. This similarity in temperatures is very likely due to the great difficulty in making samples with concentrations exactly along the Alkemade to produce a pure binary system. Hence, any variation from a true binary composition leads to "ternary contamination" in samples with compositions along the 3AN·AS /H_2O line: samples will show ternary character unless they are composed of an exact 3 to 1 molar ratio of NH_4NO_3 and $(NH_4)_2SO_4$. As a result, a very small endotherm appears in the thermograms of Figure 6 corresponding to the temperature of one of the ternary eutectics. This is seen either by the smaller slope of the first endotherm, or by a change in slope of the first endotherm, both indicating overlapping endotherms. Since the indication of first melting (either a binary or ternary eutectic point) is given by the *onset* temperature of the first endotherm in a heating process, any interfering contamination in a binary sample to produce ternary characteristics disallows the determination of the binary eutectic temperature when the two eutectics are close in temperature, as is the case here. We observed this contamination in all of our binary samples; therefore, we were unable to determine the exact temperature of the ice/3AN·AS binary eutectic. However, from phase boundary temperatures near the ice/3AN·AS Alkemade, we have determined the eutectic temperature to be >253.6 K. Theoretically, the Alkemade line should be a temperature maximum on the phase boundary. Therefore, the true binary eutectic of the 3AN·AS/H2O system is a maximum along the ice/salt phase boundary.

According to our analysis, an Alkemade line does not exist between 2AN·AS and water. First, we experimentally found that 2AN·AS/water does not constitute a true binary system. Therefore, if 2AN·AS and water shared a phase boundary, an Alkemade did not intersect it. Second, we only observed two invariant points in our experiments. If an Alkemade line had existed between 2AN·AS and water, then we would have experimentally observed another invariant point in at least one of the samples run in Figure 1. Our experiments probed the whole ice/salt phase boundary, and we did not observe 2AN·AS. Therefore, an Alkemade line cannot exist between

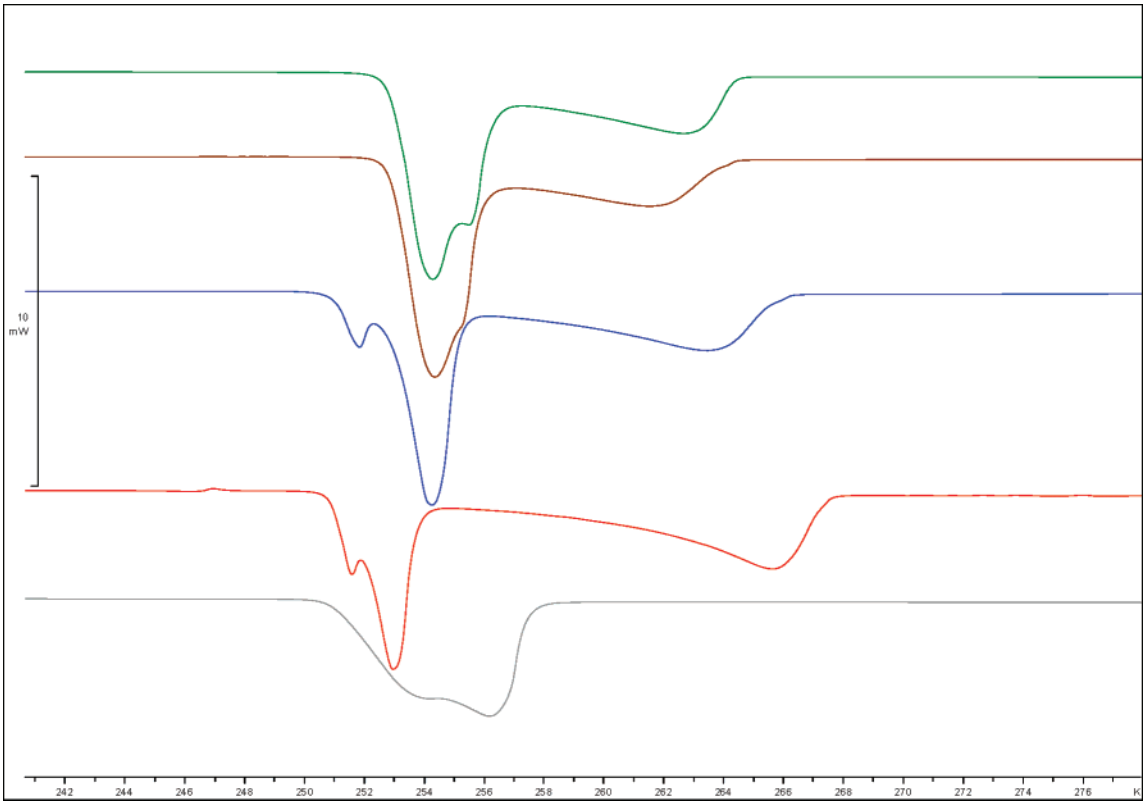

Figure 5. Thermograms used for eutectic analysis. The compositions of the thermograms are as follows: green thermogram, 20.00/7.50 wt % $NH_4NO_3/(NH_4)_2SO_4$; brown thermogram, 19.99/9.00 wt % $NH_4NO_3/(NH_4)_2SO_4$; blue thermogram, 14.99/9.99 wt % $NH_4NO_3/(NH_4)_2SO_4$; red thermogram, 10.01/10.01 wt % $NH_4NO_3/(NH_4)_2SO_4$; gray thermogram, 5.00/36.02 wt % $NH_4NO_3/(NH_4)_2SO_4$. The gray thermogram was divided by 5 for clarity. Colors of thermograms correspond to colored points and dotted lines in Figure 4 (see figure caption for details).

2AN·AS and water because ice and 2AN·AS do not share a phase boundary. We did not identify 2AN·AS in the region of the system that we studied; however, we predict that the 2AN·AS stability region is at temperatures greater than 313 K. As 2AN·AS does not share a phase boundary with ice, its phase boundary must intersect the 3AN·AS phase boundary at a temperature greater than 313 K. The intersection of the phase boundaries of 3AN·AS, 2AN·AS, and $(NH_4)_2SO_4$ forms a tributary reaction point. Point C in Figure 4 is considered a tributary reaction point because two phase boundaries meet (3AN·AS/2AN·AS and 2AN·AS/$(NH_4)_2SO_4$) with a third phase boundary (3AN·AS/$(NH_4)_4SO_4$) approaching from a lower temperature than either of the other two. As a result of the tributary reaction point, 2AN·AS cannot coexist with ice in equilibrium. When in equilibrium, 2AN·AS can only exist with liquid water.

Identification of Solids with FTIR. In our samples, crystallization and melting of ice and the various salts was detected using FTIR. An example of a typical infrared experiment of a sample with a composition on the 3AN·AS Alkemade line is given in Figure 8. As can be seen, at room temperature, the liquid has a peak at 829 cm^{-1}, most likely due to nitrate (red spectrum).[19] This sample was cooled to 230 K where both ice and 3AN·AS crystallized (black spectrum). The spectrum with the crystalline film containing ice and 3AN·AS has a doublet composed of peaks at 834 and 826 cm^{-1}. Upon warming, the 3AN·AS melted at 253 K, as indicated by the disappearance of the 834 and 826 cm^{-1} doublet and the return of the aqueous nitrate peak (blue spectrum). After the melt of 3AN·AS, ice began to melt until it completed its conversion to liquid at 258 K (green spectrum). Both of these transitions match the green thermogram with the same composition in Figure 6 with a eutectic melting temperature of 252.6 K and a final melting temperature of 258.4 K.

In an effort to confirm that the salt we observed in the FTIR spectra was in fact 3AN·AS, we produced solid 3AN·AS to acquire a spectrum of the pure solid. As previously stated in the experimental section, 3AN·AS was produced following the procedure of Smith et al.[21] Before taking a spectrum of the salt, we determined its anion ratio. Anion analysis using an ion chromatograph showed that the molar ratio of NO_3^-/SO_4^{-2} in the crystals was 3.10 ± 0.17. Therefore, the salt we crystallized had the right NO_3^-/SO_4^{2-} molar ratio to be 3AN·AS. The salt was then used to acquire an infrared spectrum in order to confirm that the peaks at 835 and 826 cm^{-1} in the 3AN·AS/H_2O samples also appeared in our crystallized 3AN·AS sample. The resulting spectra in the region of interest of solid 3AN·AS, ammonium nitrate, and ammonium sulfate (all in KBr pellet) are found in Figure 9. Additionally, the relevant region of a frozen 31.0/17.1 wt % $NH_4NO_3/(NH_4)_2SO_4$ sample is shown in the figure. The pure crystal 3AN·AS (blue) spectrum agrees with our frozen sample spectrum (with a composition along the 3AN·AS/H_2O line [red]) not only in the energies of the peaks observed (832 and 826 cm^{-1} vs 835 and 826 cm^{-1}), but also the ratio of the peak amplitudes. (We believe there is a slight shift in the 832 cm^{-1} peak of the pure 3AN·AS crystals to 835 cm^{-1} in our spectrum due to the presence of ice.) Also, it is seen that the salt we made could not have been a mixture of solid ammonium nitrate and ammonium sulfate in a ratio of 3 to 1 because the spectra of each solid cannot be added to match the observed 3AN·AS spectrum.

Recently, the infrared spectrum of each double salt, 3AN·AS and 2AN·AS, has been characterized by Schlenker et al.[26,30]

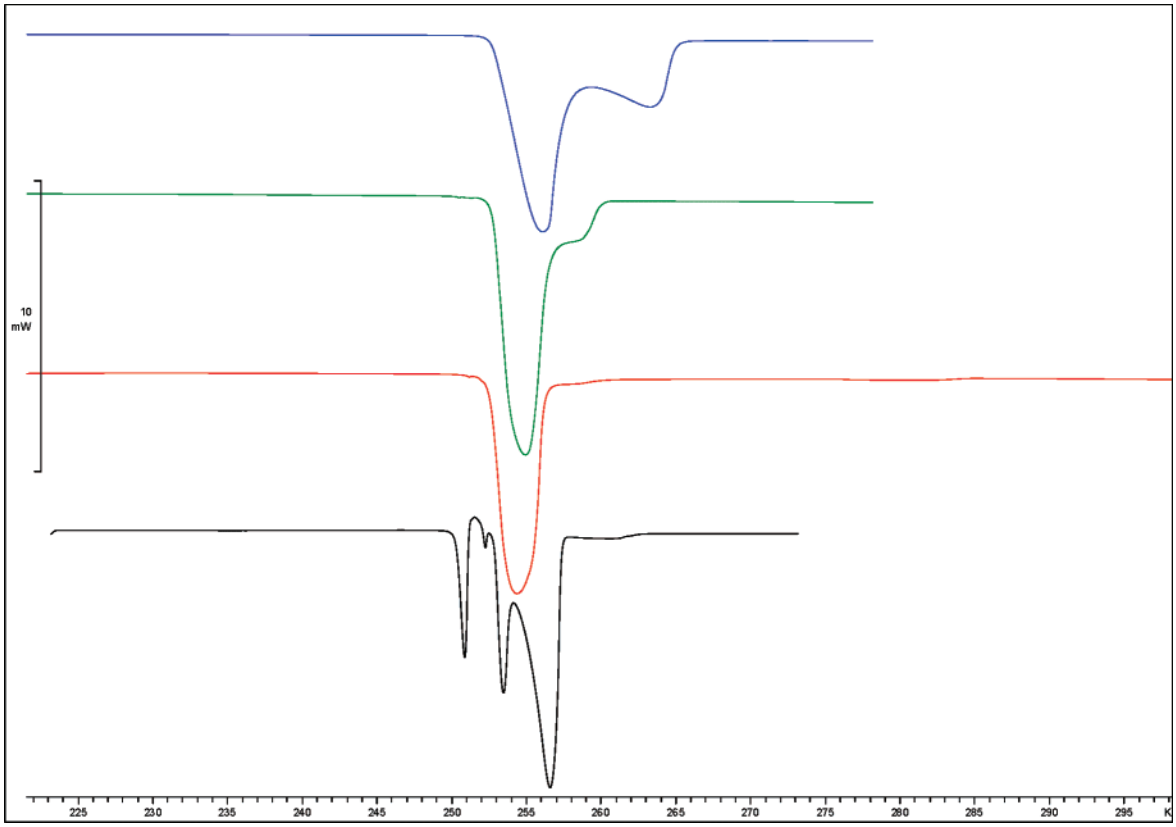

Figure 6. Thermograms for the 3AN·AS/H_2O binary system and thermal decomposition of the unknown solid. The compositions of the samples are as follows: blue thermogram, 17.49/9.63 wt % $NH_4NO_3/(NH_4)_2SO_4$; green thermogram, 22.78/12.52 wt % $NH_4NO_3/(NH_4)_2SO_4$; red thermogram, 34.70/19.09 wt % $NH_4NO_3/(NH_4)_2SO_4$; black thermogram, 39.98/5.00 wt % $NH_4NO_3/(NH_4)_2SO_4$. The black thermogram shows the decomposition of a new solid and was multiplied by 2 for the purpose of clarity.

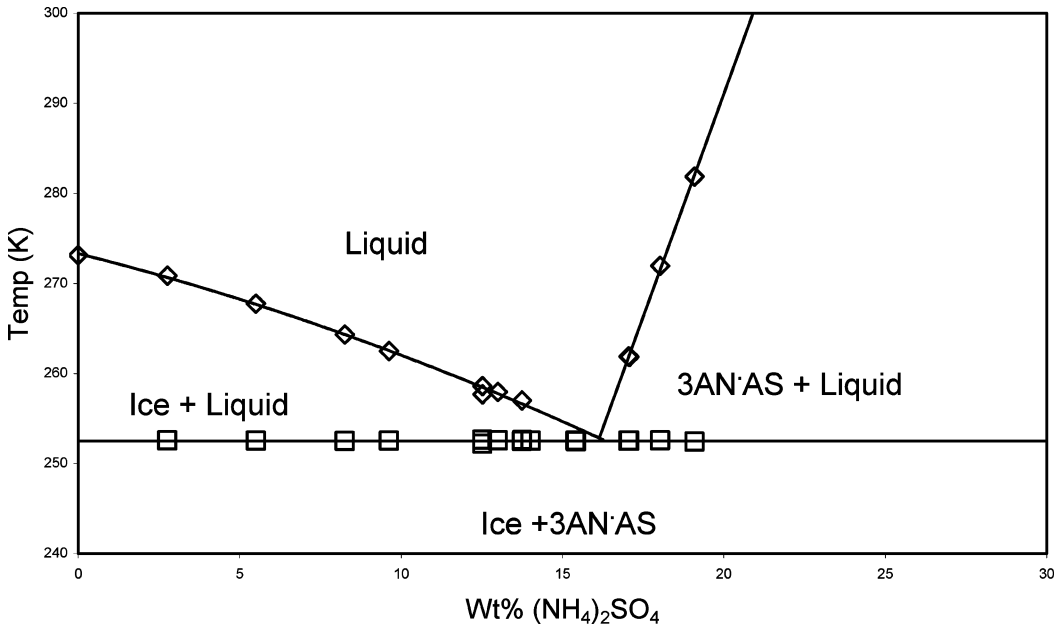

Figure 7. Experimentally determined 3AN·AS/H_2O Binary Phase diagram. The symbols are as follows: squares, eutectic melt; diamonds, final melt or dissolution.

using an aerosols flow tube technique. They assigned unique peaks characteristic of 2AN·AS to be 825 and 834 cm^{-1}, while the unique peak for 3AN·AS was found to be 821 cm^{-1}. However, we observed 826 and 832 cm^{-1} to be peaks characteristic of anhydrous 3AN·AS, not 2AN·AS, and we have not observed a peak at 821 cm^{-1} for 3AN·AS as Schlenker et al. have. They state the uncertainty in their peak measurements to be ± 3 cm^{-1}, and ours is likely of the same magnitude. These uncertainties may account for the difference between their observations of 821 versus ours of 826 cm^{-1} for 3AN·AS; however, it does not account for our observation of a peak at 832 cm^{-1} for 3AN·AS, which they assign to 2AN·AS. Schlenker et al. do not give justification for their assignments or how they determined the exact composition of the solids they observed

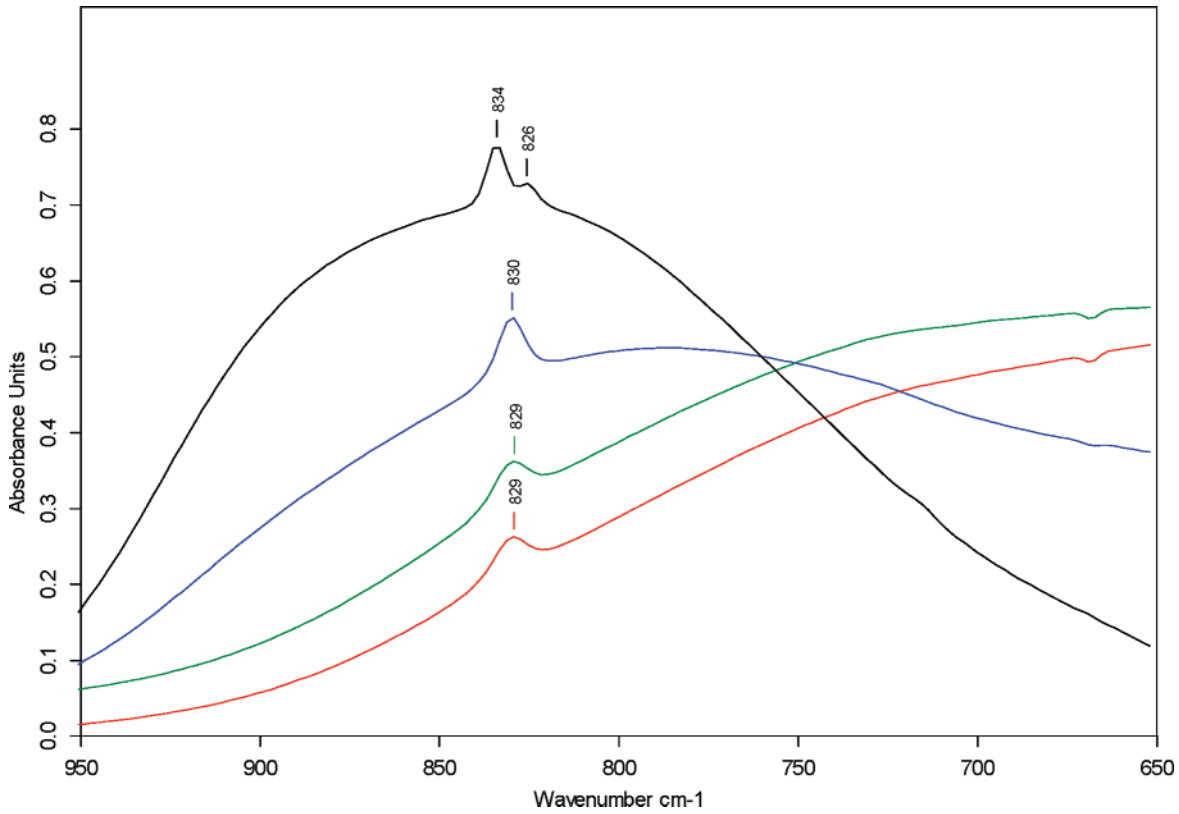

Figure 8. IR spectra of a 22.78/12.52 $NH_4NO_3/(NH_4)_2SO_4$ sample: red, completely liquid sample at 284 K; black, crystallization of both ice and 3AN·AS occurs at 230 K; blue, the eutectic melt of 3AN·AS occurs while at 253 K; green; the melting of ice has completed and only liquid remains at 258 K. Red spectrum is offset by −0.05 absorbance units for clarity.

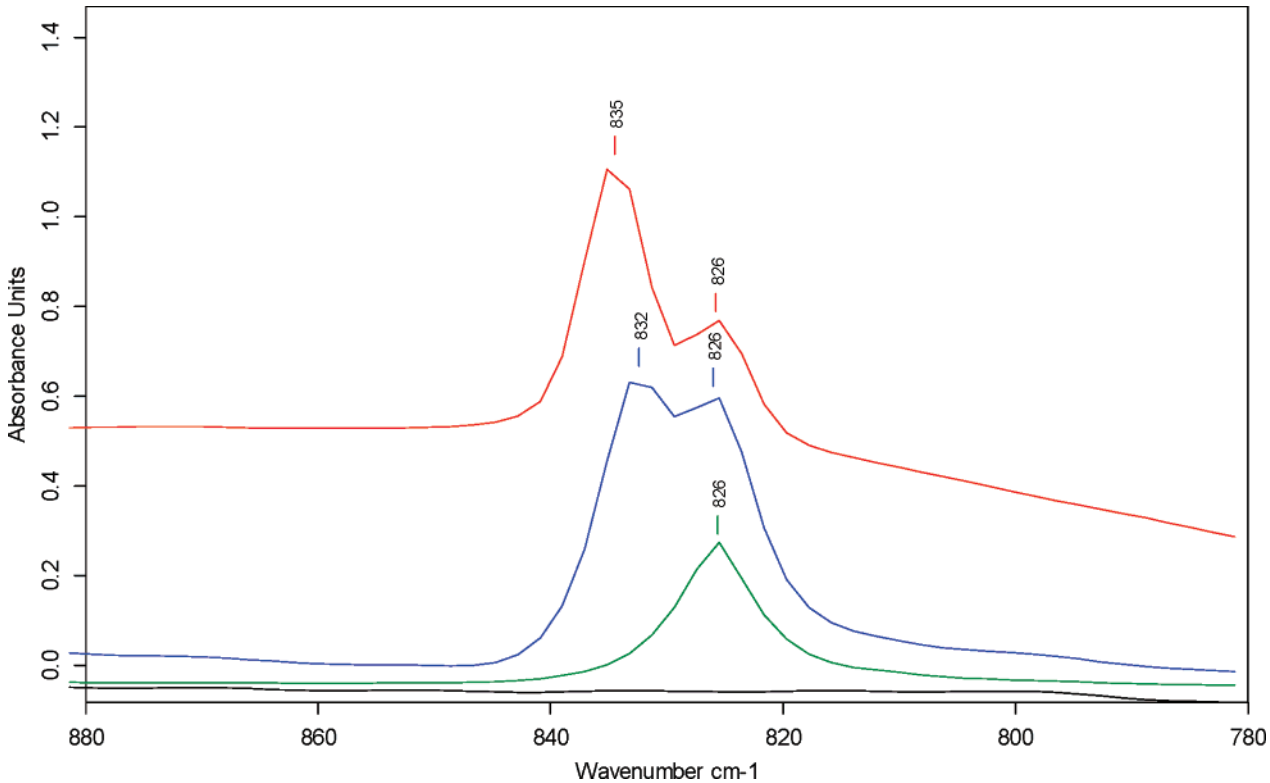

Figure 9. Infrared spectra of salts: black, $(NH_4)_2SO_4$; green, NH_4NO_3; blue, 3AN·AS crystallized according to the method of Smith et al.;[21] red, solid ternary sample (31.0/17.1 wt % $NH_4NO_3/(NH_4)_2SO_4$). The spectra were offset for clarity as follows: Black: +0.35 units, Green: Divided by 8, Blue: +0.3 units, Red: Multiplied by 6 and +0.14 units. Additionally, ice was subtracted from the ternary spectrum.

in their studies. As stated above, we obtained a reference spectrum for 3AN·AS by producing crystals of the solid using the procedure of Smith et al.,[21] and confirmed the composition by ion chromatography. Therefore, we are confident in our conclusion that the doublet at 826 and 832 ± 3 cm^{-1} is characteristic of 3AN·AS.

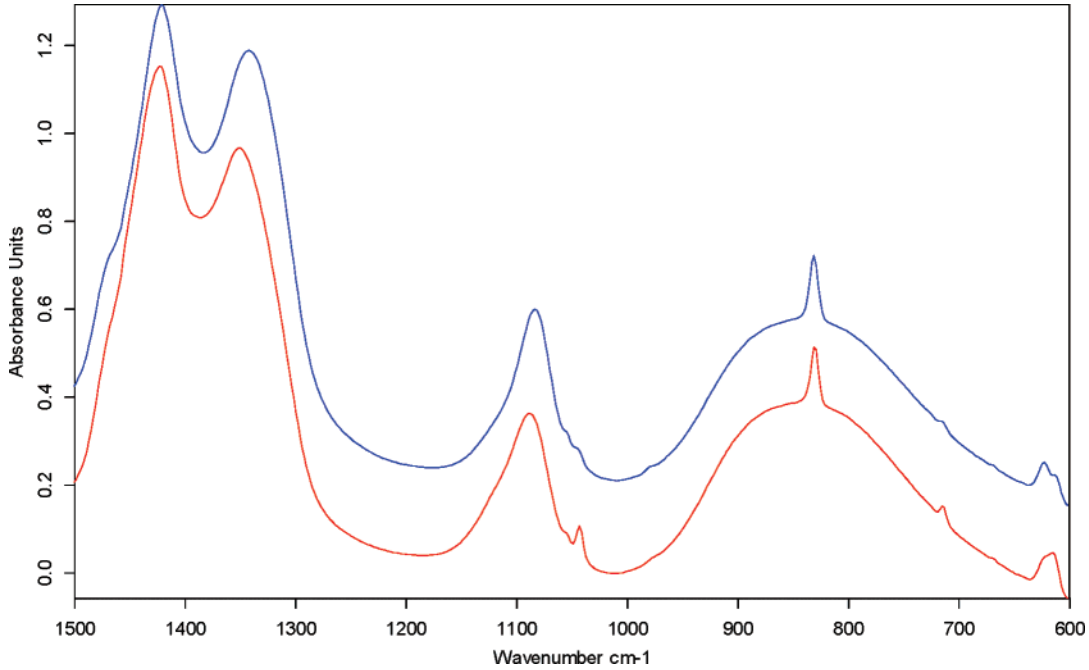

Figure 10. Infrared spectra of a new solid before and after thermal decomposition at 250 K in a 39.98/10.00 wt % $NH_4NO_3/(NH_4)_2SO_4$ sample. Red, new solid present in frozen sample at 247 K; blue, after solid decomposed at 250 K.

Mixed Solid. We have observed the thermal decomposition of a previously unreported solid in 42 of our samples at a temperature of 250.82 ± 0.31 K, as determined by DSC. The black thermogram, in Figure 6, with a concentration of 39.98/5.00 wt % $NH_4NO_3/(NH_4)_2SO_4$ shows an example of the decomposition of this solid. The thermal decomposition is immediately followed by a recrystallization, because the liquid is unstable at a temperature below the ternary eutectic. As three endotherms follow in the thermogram at the predicted temperatures, it is apparent that the recrystallization returns the solids in the sample to those that compose the Alkemade region in which the sample is present.

We also observe a peak in the infrared spectrum that appears to be characteristic of the new solid (see Figure 10.) Samples that undergo the thermal decomposition at 250 K have a peak that disappears at 1043 cm^{-1} as is seen in Figure 10. Additionally, the amplitude of the NH_4^+ peak at 1426 cm^{-1} typically decreases, the NO_3^- peak at 1350 cm^{-1} shifts slightly to 1342 cm^{-1}, the SO_4^{2-} peak at 1089 cm^{-1} shifts slightly to 1084 cm^{-1}, and the SO_4^{2-} peak at 619 cm^{-1} changes shape upon thermal decomposition of the solid. Each sample that underwent this thermal decomposition is labeled in Figure 1.

From our DSC and IR experiments, we observed that all but one of the samples that underwent the thermal decomposition were located in the NH_4NO_3/3AN·AS/ H_2O Alkemade region (no samples with NH_4NO_3 concentration below 30 wt % had this transition, whereas most samples above 40 wt % NH_4NO_3 exhibited this transition.) Additionally, the amount of sample undergoing this transition increased with increasing $(NH_4)_2SO_4$ concentration in the stated region. However, there does not appear to be a more specific trend such that we could assign a possible composition and mole ratio of $NH_4NO_3/(NH_4)_2SO_4$ to the solid. Given the range of $NH_4NO_3/(NH_4)_2SO_4$ ratios in the NH_4NO_3/3AN·AS/H_2O Alkemade region, we believe the solid could be 4AN·AS or a combined salt that is richer in ammonium nitrate than the known combined salts. Further investigation of this solid is needed to more precisely determine its nature and properties.

There is a known solid/solid-phase transition of NH_4NO_3 from tetragonal to orthorhombic configurations at 256.2 K with an enthalpy of transition of 473 J/ mol.[31] The average enthalpy of the transition we observe is 5.6 kJ/mol and occurs at a temperature of 250 K, well over a factor of 10 larger in energy and 6 K lower in temperature than the pure NH_4NO_3 transition. Also, we note that the amount of solid in this phase scales with $(NH_4)_2SO_4$ concentration, and the IR spectrum contains shifts in sulfate peaks when this solid decomposes. Neither of these observations would be seen if the transition we observe were simply due to the solid/solid-phase transition of ammonium nitrate. Therefore, we conclude it is highly unlikely that the transition we observe is the tetragonal to orthorhombic transition of ammonium nitrate.

Comparison to AIM. We have compared our experimentally determined melting points to the predictions made by the Aerosol Inorganics Model (AIM).[20] The model is based on solid/liquid equilibrium data for the NH_4NO_3/H_2O and $(NH_4)_2SO_4/H_2O$ binary systems down to the eutectic temperatures. However, for ternary components, the model is based on literature data from 273.15 K and above. Therefore, we expect the model to perform best at low ternary solute concentrations, which fall within the ice primary phase field.

The results of the comparison between our final melting point data and those predicted by the AIM are found in Figure 11. The range of the difference in temperature between our data and that calculated by the AIM model is −44 to +8 K; however, very few predictions deviated from our data as significantly as the maximum and minimum of the range. We calculated the average absolute difference in final melting and dissolution temperatures to be ±2.6 K; thus, the model performs quite well at lower temperatures even though it is based on data at higher temperatures. Inside the ice primary phase field, the majority of the predictions made by the AIM are within 1 K of our experimentally observed final melting points. The area of the phase diagram with the largest deviation between our data and the predictions of the AIM model is outside of the ice primary phase field.

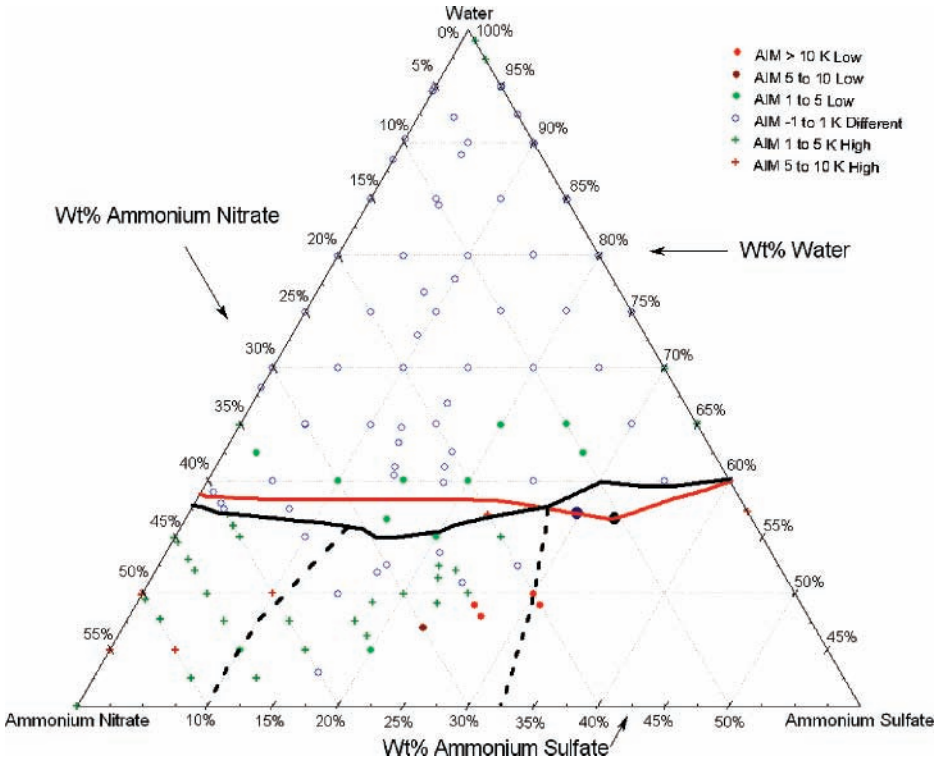

Figure 11. Difference between AIM predictions and our experimental data in K (our data—AIM prediction). The thick red line is the ice/salt phase boundary predicted by the AIM model while the black lines are our experimentally determined phase boundaries. The large solid blue and black points are the AIM's predicted ternary eutectics composed of NH_4NO_3/3AN·AS/H_2O and 3AN·AS/$(NH_4)_2SO_4$/H_2O, respectively.

The discrepancies in the salt primary phase fields are the most significant. This is most likely due to the difference in the locations of the primary phase fields predicted by the AIM. The AIM predicts 2AN·AS to be a stable solid inside our defined 3AN·AS primary phase field, whereas the only salts that we observed in this region were NH_4NO_3 and 3AN·AS. However, the AIM model agrees with our experimental results as it predicts that ice and 2AN·AS do not share a phase boundary. Additionally, the AIM predicts two ternary eutectics composed of NH_4NO_3/3AN·AS/H_2O (13.1/29.8 wt % NH_4NO_3/$(NH_4)_2SO_4$) and 3AN·AS/ $(NH_4)_2SO_4$/H_2O (10.5/32.9 wt % NH_4NO_3/$(NH_4)_2SO_4$) with melting temperatures of 252.0 and 251.3 K, respectively. Although the solids of the ternary eutectics are in agreement with our study, the predicted composition of the NH_4NO_3/3AN·AS/H_2O ternary eutectic point differs significantly from observation, as seen in Figure 11.

Summary

The water-rich region of the NH_4NO_3/$(NH_4)_2SO_4$/H_2O system has been investigated at low temperatures. We coupled our experimental data with literature data to create an NH_4NO_3/$(NH_4)_2SO_4$/H_2O solid/liquid phase diagram. We have demonstrated that an Alkemade line exists between 3AN·AS and H_2O; therefore, the NH_4NO_3/$(NH_4)_2SO_4$/H_2O system can be broken into two Alkemade regions which act as individual ternary systems. These Alkemade regions are composed of NH_4NO_3/3AN·AS/H_2O and 3AN·AS/$(NH_4)_2SO_4$/H_2O with ternary eutectic points at 32.0/13.0 ± 2.0 and 16.0/26.0 ± 2.0 wt % NH_4NO_3/$(NH_4)_2SO_4$ and melting temperatures of 252.53 ± 0.37 and 251.11 ± 0.48 K, respectively. In addition to demonstrating the existence of these Alkemade regions, we have determined that 3AN·AS/H_2O is a true binary system, and hence it shares a phase boundary intersected by the Alkemade. Additionally, we have directly observed 3AN·AS using infrared spectroscopy. The solid found in the 3AN·AS/H_2O absorption spectrum was matched to solid 3AN·AS that we crystallized following the procedure of Smith et al.,[21] and we report a unique peak due to 3AN·AS at 832−835 cm^{-1}. The thermal decomposition of a new solid at 250.82 ± 0.31 K has been reported. We observed this decomposition in both our infrared spectroscopy and our DSC data. The transition was observed in all samples with concentrations lying in the salt primary phase fields of the NH_4NO_3/3AN·AS/H_2O Alkemade region (with one exception). Samples that formed the new solid where rich in ammonium nitrate and poor in ammonium sulfate; therefore, we believe the solid is another combined salt that is richer in ammonium nitrate than 3AN·AS.

We have also compared our data to the predictions of the Aerosol Inorganics Model (AIM).[20] The AIM model is based on solubility and electrodynamic balance data above 273 K; as a result, any predictions below 273 K are an extrapolation of the solubility and other data. It was found that the AIM's predictions for final melting and dissolution temperatures were in good agreement with our experimental data, particularly in the ice primary phase field. We also found good agreement between our experimentally determined ice/salt phase boundary and the AIM model's prediction. The AIM predicts two ternary eutectic points consisting of the same solids but with differing compositions than our reported ternary eutectics. Also, the AIM model predicts that 2AN·AS is a stable salt in the region that we studied, although we did not observe 2AN·AS in any of our experiments.

It is well known that both 2AN·AS and 3AN·AS exist.[15] However, we have experimentally shown that 2AN·AS does not form in the presence of ice when in equilibrium, and therefore, they do not share a phase boundary. We have determined the 2AN·AS primary phase region exists at tem-

peratures above 313 K; as a result, it is possible for 2AN·AS to coexist with solution, but not ice.

Acknowledgment. This work was supported by the NSF Atmospheric Chemistry Program (ATM-0442273).

Supporting Information Available: Table 1S contains the experimentally determined melting temperatures for the $NH_4NO_3/(NH_4)_2SO_4/H_2O$ system used to create Figure 5. This material is available free of charge via the Internet at http://pubs.acs.org.

References and Notes

(1) Mason, B. J. *The Physics of Clouds*; Oxford University Press: New York, 1957.

(2) Warneck, P. *Chemistry of the Natural Atmosphere*, 2nd ed.; Academic Press: San Diego, 2000; pp 405−428.

(3) Talbot, R. W.; Dibb, J. E.; Loomis, M. B. *Geophys. Res. Lett.* **1998**, *25*, 1367−1370.

(4) Tabazadeh, A.; Toon, O. B. *Geophys. Res. Lett.* **1998**, *25*, 1379−1382.

(5) Martin, S. T. *Geophys. Res. Lett.* **1998**, *25*, 1657−1660.

(6) Cziczo, D. J.; Abbatt, J. P. D. *J. Geophys. Res.* **1999**, *104*, 13,-781−13,790.

(7) Bertram, A. K.; Koop, T.; Molina, L. T.; Molina, M. J. *J. Phys. Chem. A* **2000**, *104*, 584−588.

(8) Chelf, J. H.; Martin, S. T. *J. Geophys. Res.* **2001**, *106*, 1215−1226.

(9) Prenni, A. J.; Wise, M. E.; Brooks, S. D.; Tolbert, M. A. *J. Geophys. Res.* **2001**, *106*, 3037−3044.

(10) Martin, S. T. *Chem. Rev.* **2000**, *100*, 3403−3453.

(11) Seinfeld, J. H.; Pandis, S. N. *Atmospheric Chemistry and Physics*; Wiley: New York, 1998; pp 440−446.

(12) Martin, S. T.; Hung, H.-M.; Park, R. J.; Jacob, D. J.; Spurr, R. J. D.; Chance, K. V.; Chin, M. *Atmos. Chem. Phys.* **2004**, *4*, 183−213.

(13) Hu, J. H.; Abbatt, J. P. D. *J. Phys. Chem. A* **1997**, *101*, 871−878.

(14) Wahner, A.; Mentel, T. F.; Sohn, M.; Stier, J. *J. Geophys. Res.* **1998**, *103* (D23), 31103−31112.

(15) Silcock, H. L. *Solubilities of Inorganic and Organic Compounds*; Pergamon: Oxford, 1979; Vols. 1 and 3.

(16) Timmermans, J. *The Physico-Chemical Constants of Binary Systems in Concentrated Solutions*, Interscience: New York, 1960; pp 602−604, 619−621.

(17) Linke, W. F. *Solubilities of Inorganic and Metal-Organic Compounds*; American Chemical Society: Washington, DC, 1965; Vol 2, p 755.

(18) Perman, E. P.; Howells, W. J. *J. Chem. Soc.* **1923**, *123*, 2128−2134.

(19) Bowen, N. L. *J. Phys. Chem.* **1926**, *30*, 736−737.

(20) Wexler, A. S.; Clegg, S. L. *J. Geophys. Res.* **2002**, *107* (D14), http://dx.doi.org/10.1029/2001JD000451.

(21) Smith, J. P.; Lehr, J. R.; Frazier, A. W. *J. Agric. Food Chem.* **1962**, *10*, 77−78.

(22) Zhang, R.; Wooldridge, P. J.; Abbatt, J. P. D.; Molina, M. J. *J. Phys. Chem*. **1993**, *97*, 7351−7358.

(23) Lide D. R. ed. CRC *Handbook of Chemistry and Physics*, 74th Ed.; CRC Press: Boca Raton, 1993; 3−208, 351, 356−358.

(24) Bertie, J. E.; Labbe, H. J.; Whalley, E. *J. Chem. Phys.* **1969**, *50*, 4501.

(25) Pouchert, C. J. *The Aldrich Library of FT-IR Spectra*; Aldrich: Milwaukee, 1997; pp 4751, 4736.

(26) Schlenker, J. C.; Malinowsk, A.; Martin, S. T.; Hung, H.; Rudich, Y. *J. Phys. Chem. A* **2004**, *108*, 9375−9383.

(27) Miller, F. A; Wilkins, C. H. *Anal. Chem*. **1952**, *24*, 1253−1294.

(28) Beyer, K. B.; Bothe, J. R.; Burrmann, N. *J. Phys. Chem. A* **2007**, *111*, 479−494.

(29) Ehlers, E. G. *The Interpretation of Geological Phase Diagrams*; Dover: Mineola, NY, 1972; p 42.

(30) Schlenker, J. C.; Martin, S. T.; *J. Phys. Chem. A* **2005**, *109*, 9980−9985.

(31) Nagatani, M.; Seiyama, T.; Sakiyama, M.; Suga, H.; Seki, S. *Bull. Chem. Soc. Jpn* **1967**, *40*, 1833−1844.